Performance of a directly deposited optical blocking filter on x-ray CCDs: case study from the REgolith X-ray Imaging Spectrometer (REXIS) experiment

Performance of a directly deposited optical blocking filter on x-ray CCDs: case study from the REgolith X-ray Imaging Spectrometer (REXIS) experiment

Carolyn Thayer,[a] Rebecca Masterson,[a,*] Branden Allen,[b] Kevin Ryu,[c] Marshall W. Bautz,[a] Solan Megerssa,[a] Mark Chodas,[a] David Guevel,[b] Daniel Hoak,[b] Jaesub Hong,[b] Madeline Lambert,[a] Jonathan Grindlay,[b] and Richard P. Binzel[a]

[a]Massachusetts Institute of Technology, Cambridge, Massachusetts, United States
[b]Harvard University, Harvard-Smithsonian Center for Astrophysics, Cambridge, Massachusetts, United States
[c]Lincoln Laboratory, Lexington, Massachusetts, United States

Abstract. The REgolith X-ray Imaging Spectrometer (REXIS) is a soft x-ray spectrometer and the student collaboration instrument aboard NASA's OSIRIS-REx asteroid sample return mission. REXIS utilizes MIT Lincoln Laboratory CCID-41 x-ray detectors coated with a directly deposited optical blocking filter (OBF) with a thickness of 320 nm. The aluminum coating, developed at MIT Lincoln Laboratory, is designed to block visible light from the detector, to maintain high sensitivity to soft x-rays in the presence of reflected sunlight from the surface of the target asteroid Bennu. The scientific objective for the REXIS instrument is to measure the stimulated x-ray flux fluoresced from Bennu to discern elemental abundances present on the asteroid's surface. The coating technique applied for blocking visible light had not previously been used on the CCD-41s in an extended space flight mission. The performance of the OBF on the flight detectors was not characterized before and after environmental stress testing. Therefore, to mature the OBF to technology readiness level (TRL) 6, the flight spare detectors were tested while the instrument was on the way to the asteroid. The flight spare hardware underwent vibration and thermal environmental stress testing to test the durability and effectiveness of the OBF. This testing informed our expectations of the in-flight OBF once it reached the asteroid and helped mature the TRL level of this directly deposited OBF. We discuss the setup and results of those tests and address the performance of the flight OBF at the asteroid. We conclude that depositing an aluminum OBF onto the surface of a charge-coupled device is able to withstand stresses of launch and an extended life-mission in interplanetary space. [DOI: 10.1117/1.JATIS.7.4.046001]

Keywords: REXIS; OSIRIS-Rex; soft x-rays; optical blocking filter; charge-coupled devices.

Paper 21067 received Jun. 17, 2021; accepted for publication Dec. 1, 2021; published online Dec. 22, 2021.

1 Introduction

The REgolith X-ray Imaging Spectrometer (REXIS) is the student collaboration instrument aboard NASA's OSIRIS-REx asteroid sample return mission. OSIRIS-REx is a NASA New Frontiers mission designed to study the near-Earth asteroid Bennu and return to Earth with a sample of the asteroid regolith.[1] REXIS, shown in Fig. 1, is a coded-aperture x-ray spectrometer designed to measure soft x-rays fluoresced from the asteroid in the range 0.5 to 7.5 keV to map the relative elemental abundances in the regolith layer of Bennu and categorize it among the major meteorite groups.[2] REXIS consists of two assemblies: the main spectrometer and a solar x-ray monitor (SXM). The SXM measures the solar x-ray activity to characterize the level of x-ray flux the asteroid is receiving and therefore calibrate the resulting stimulated fluorescence.

*Address all correspondence to Rebecca Masterson, becki@mit.edu

2329-4124/2021/$28.00 © 2021 SPIE

Fig. 1 Fully assembled REXIS flight instrument awaiting integration to the OSIRIS-REx spacecraft.

The REXIS main spectrometer has a coded-aperture mask at the flux entrance with detectors 19.9 cm below the mask. The detector assembly consists of four silicon wafer charge-coupled devices (CCD) arranged in a two-by-two array. The devices are CCID-41 detectors developed at MIT's Lincoln Laboratory, each containing 1024×1024 pixels that are 24×24 μm in dimension. The energy sensitivity of the CCID-41 is ideal for detecting the fluorescence of key elements of interest, such as Fe, Mg, and S. Because the CCDs are sensitive to both x-ray and optical photons, it is necessary to block the visible wavelengths of solar radiation reflecting off the asteroid that contribute significantly as a source of noise in the REXIS data. An optical blocking filter (OBF) comprised of a 320-nm-thick aluminum film directly deposited onto the detector surface with a technique devised at MIT Lincoln Laboratory (LL) is used to reduce the intensity of the visible light that interacts with the CCDs while allowing the soft x-rays of interest to be detected.[3]

A team working at LL developed the technique of directly depositing an OBF on a CCD as part of a NASA's Strategic Astrophysics Technology Program grant with the aim to replace the commonly used fragile, free-standing blocking filters. When REXIS was selected as an instrument for the OSIRIS-REx mission, it presented an opportunity for a technology development program for this untested OBF technology. The first iteration of the OBF was 220-nm thick, and testing described in Ref. 3 showed that a significant flux of visible light was nonetheless being transmitted through the OBF. It was determined that microscopic pinholes in the surface of the deposited aluminum likely caused by particles and roughness on the silicon substrate upon which the OBF was deposited were letting through extra light. The amount of light that passed through the pinholes in the first iteration of the OBF was high enough that REXIS would not be able to meet all of its science requirements. The two requirements that were not met are

1. The percentage of detector area made unavailable for data collection due to pinholes in the OBF shall be $< 0.75\%$.
2. The OBF shall reduce the flux of photons between 100 and 10,000 nm that encounter the CCD top surface such that less than 1e-5% of photons in that band are detected by the CCD.

To mitigate this light leak, an additional 100-nm layer of aluminum was applied, bringing the total thickness to 320 nm and significantly reducing the number of pinholes observed in the REXIS CCDs.[3] Even with this additional layer, further performance characterization showed that light also leaked through the edges and the backside of the CCD, so both black paint and OBF coating were applied to these areas as well.

Although directly deposited OBFs have been flown previously,[4,5] REXIS is the first NASA x-ray spectrometer to fly this type of coating for planetary observation using Lincoln Laboratory CCDs and deposition techniques.[6] Because REXIS was developed as a student instrument with a minimal budget, the performance of the OBF on the flight detectors could not be characterized during the prelaunch environmental testing. Therefore, after launch and during the 2-year cruise to the asteroid Bennu, environmental stress tests as defined in NASA's General Environmental Standards (GEVS)[7] were performed on the flight spare detector assembly mount (DAM) to predict if there would be any degradation in the OBF performance due to launch. Postlaunch ground tests of the flight spare that validate the OBF performance provide a system demonstration in a relevant environment, raising the NASA technology readiness level (TRL)[8] to 6. Good performance of the module in flight demonstrates that the system is flight proven through successful mission operations and raises the TRL to 9. In this paper, we discuss both the process and results of the environmental tests and the performance of the OBF in flight when observing the asteroid in the presence of optical light.

2 Ground Testing Methods

This section details the ground tests performed on the flight spare DAM to fully characterize the performance of the OBF before and after exposure to flight-like environments. A flowchart of the test procedure is shown in Fig. 2. Initial light leak tests, the first two blocks in the flow, were performed at −70°C to characterize the pixels affected by pinholes in the OBF and to verify that the OBF met the REXIS mission requirements. Note that the pinholes are much smaller than the CCD pixels, so a single pixel may show elevated charge due to leak from one of more pinholes. In this paper, when discussing the test results, we use the term pinhole to describe any pixel that shows elevated charged due to one of more OBF pinholes. Next the DAM underwent a vibration test followed by additional light leak tests to identify any changes to the OBF. Next, the DAM was cooled down to −90°C and another set of light leak tests were performed. The DAM was then brought back to room temperature, rotated 180 deg (to evaluate the sensitivity of the stray light environment to orientation), and cooled down to −70°C for additional light leak tests. A final light leak test was preformed with the same conditions as the initial light leak tests. Throughout this test campaign, the DAM experienced 10 thermal cycles from 20°C (or warmer) to −70°C (or colder). Eight of these 10 cycles occurred between the first and last light leak tests. The OBF performance was evaluated by comparing data from the first and last light leak tests to determine if there was any change due to thermal stress. All thermal cycles were conducted at −70°C or colder, because the required operating temperature for the REXIS CCDs is −60°C. In

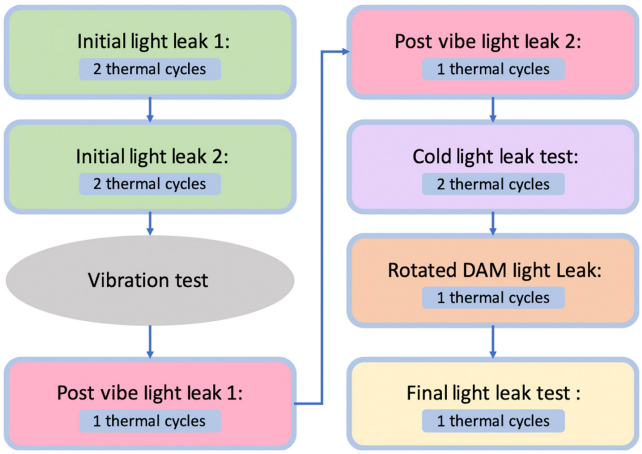

Fig. 2 Light leak testing flow diagram. All rectangles are light leak tests and the different colors note different stages of testing. The oval is the vibration test. For each test, it is noted how many times the DAM was thermally cycled.

general, colder temperatures allowed for better measurement of light leak due to the reduction in dark current. The cycle limits were chosen to encompass the REXIS operating range with 10°C of margin.

2.1 *OBF Performance Assessment Criteria*

The initial light leak test was used to assess the performance of the OBF to verify that it meets the instrument requirements and to provide a baseline before environmental testing. For the purpose of comparing the requirements to testing, both the previous testing done by LL and the testing described in this paper, the large area optical performance (LAOP) and the pixel optical density (POD) are characterized for each CCD. LAOP is calculated by counting the number of pixels in which optical light bleed-through is observed above the noise floor, N_b, in areas that are directly illuminated with visible light. POD is the measure of the reduction in visible flux registered by the CCD due to the OBF and is calculated for all illuminated pixels by dividing the number of expected incident photons, N_i, (accounting for the Gaussian beam intensity) by the number of detected photons, N_d, for each pixel:

$$\text{LAOP} = N_b, \tag{1}$$

$$\text{POD} = \frac{N_i}{N_d}. \tag{2}$$

Here, we adopt the conventional definition of optical density as the common logarithm of the ratio of incident to detected photon flux. The lower the POD value for a pixel, the larger the fraction of incident light that made it through the OBF. In order for REXIS to meet its science requirements, LAOP must be less than 1% of the illuminated area and the fraction of pixels with a POD <7 must be less than 1% of the illuminated area.

After environmental tests, the stability of the OBF performance was evaluated to ensure that the OBF did not deteriorate due to exposure to vibration and thermal cycling. A deterioration in performance, even if still within requirements, puts the durability of the OBF over the course of a long-duration mission into question. The following success criteria for comparison between tests done before and after environmental testing are used:

- Postenvironmental testing, LAOP per CCD should not increase by more than 2σ, where σ is the observed standard deviation derived from multiple measurements.
- Postenvironmental testing, the fraction of illuminated pixels with POD <7 per CCD should not increase by more than 2σ, where σ is the observed standard deviation derived from multiple measurements.

The criteria of 2σ were chosen to provide a measure tighter than the requirements to assess variability.

2.2 *Light Leak Test*

For the light leak test, the REXIS flight spare DAM was installed in a thermal vacuum chamber with an optical fiber suspended a few inches above the CCDs, positioned so that it directly illuminated portions of all four CCDs. Figure 3 shows the setup of the REXIS tower with the CCDs inside. The figure on the right shows the view inside the tower with the optical fiber positioned to shine on the four CCDs directly below. Figure 4 shows a schematic view of the illuminated area on the CCD array. Note that the illuminated portion of the CCDs is offset from the geometrical center of the array. The optical fiber was fed out of the chamber and attached to a 637-nm laser source. The mount for the fiber also held two ^{55}Fe sources that were always present whether or not the laser source was turned on. The laser and fiber setup for the light leak test were calibrated with a photodiode to determine the flux of the optical light on the detectors. The end of the fiber was not terminated, so the spread of the light coming out could be modeled with a Gaussian intensity distribution to calculate the incident light on the detectors. A basic geometrical approximation that takes into account the Gaussian nature of the output beam is used as the

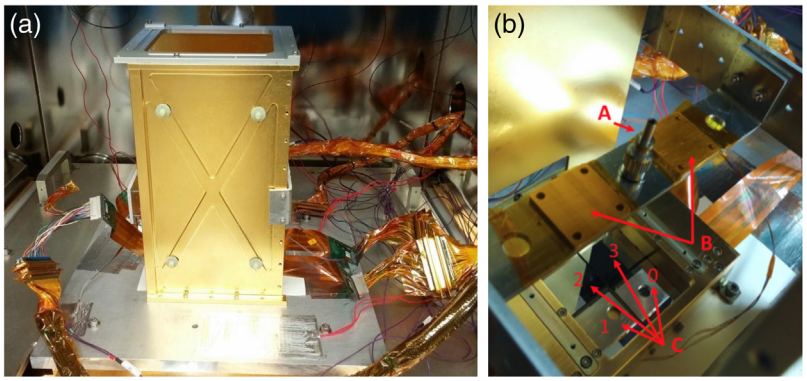

Fig. 3 (a) The REXIS spare tower in the vacuum chamber, the DAM is inside the tower at the bottom. The tower supports the optical fiber and the x-ray source. (b) The view inside the tower showing the end of the optical fiber positioned above the CCDs (A), the ^{55}Fe sources (B), and the four CCDs in the DAM with their numbering convention (C).

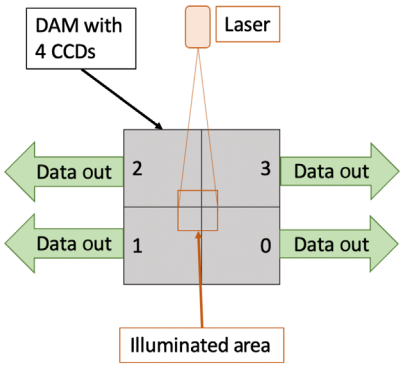

Fig. 4 Schematic showing the illuminated area on the CCDs during the light leak test. Note that the illuminated area is offset from the geometric center of the CCD array.

intensity scaling function for incident light on the detectors. The intensity scaling function I/I_0 is a function of distance from the beam axis (r) and is governed by Eq. (3):

$$\frac{I}{I_0}(r) = e^{\frac{-2r^2}{w_0^2}}, \tag{3}$$

$$w_0 = \tan(\arcsin(\alpha)) * z. \tag{4}$$

The Gaussian beam radius, w_0, is the radius at which the intensity drops to $1/e^2$ of its peak value and is computed using Eq. (4), where z is the distance from the detector to the end of the fiber optic cable, and α is the numerical aperture of the fiber, specified by the manufacturer to be 0.12. Using a value $z \approx 47$ mm, we find w_0 in the range 5.7 mm. Given 11.0 mW power from the end of the fiber, 4-s REXIS frame integration time, and a pixel size of 24 μm, a peak intensity of light on the detector surface is calculated to be $I_0 = 1.5 \times 10^{12}$ photon/pixel/frame. The light leak test was preformed with the REXIS detector electronics and a commercial frame-grabber to allow for more efficient acquisition of full frames of data. During each light leak test, frames were collected with no optical illumination, 4.6 mW optical light, and 11.0 mW of optical light. These two illumination levels bracket the expected level of optical light levels seen by REXIS at Bennu, and the OBF performance is evaluated at each light level.

To evaluate the OBF performance from the light leak test data, the data go through the processing flow shown in Fig. 5. Pixels affected by pinholes (referred to simply as pinholes going forward) are identified at each illumination level by calculating a corrected average of 25 frames. The first step is to randomly choose 25 of the illuminated frames at a single

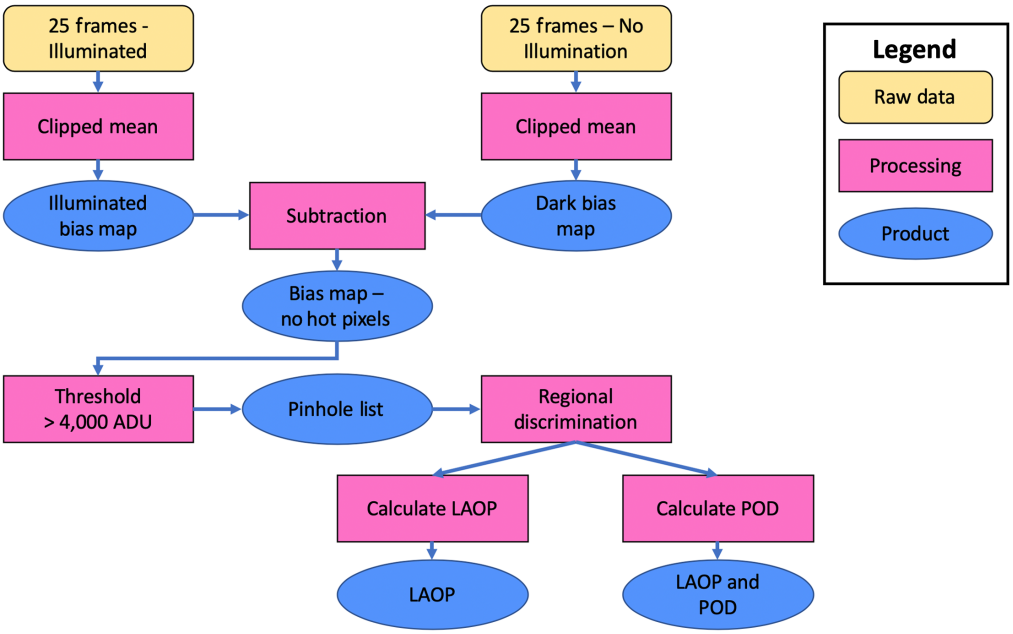

Fig. 5 Light leak data processing flow chart. A clipped mean is made from both 25 illuminates frames and 25 dark frames to make a illuminated bias map and a dark bias map. The dark bias map is subtracted from the illuminated bias map to remove any hot pixels. A threshold of 400 ADU is applied to the hot pixel-free bias map to locate all optical light events. A regional discrimination is applied to those events and the ones within the designated illuminated region are used to calculate LAOP and POD.

illumination level and create a single illuminated bias map by taking the clipped mean of the frames. The clipped mean is calculated by first removing any values that are above or below 3σ of the median pixel value and then calculating the mean of the remaining values for each pixel in the frame. Calculating the mean in this manner removes any x-ray events from the bias frame while retaining any pixels with persistent charge in all of the frames. The same process is performed on 25 frames that are taken without any illumination, i.e., dark frames, to create a dark bias map. The illuminated bias map includes all the constant elevated pixels but no x-ray events from the Fe^{55} calibration source. The dark bias map includes only hot pixels inherent to the detector. The dark bias map is subtracted from the illuminated bias map to remove all hot pixels and system noise leaving only pinhole events. Next a threshold of 4000 ADU is applied to the resulting bias map, if a pixel has a charge level at or above the threshold it is considered to have registered optical light and identified as a pinhole. The threshold was set at ~30% higher than a single pixel ^{55}Fe event to avoid counting any potential x-rays that may have made it through the bias subtraction step. The list of pinholes is then subjected to a regional discrimination because, due to the positioning of the optical fiber, only subsections of the CCDs with high enough incident light are defined as the illuminated region. There are pixels in the pinhole list that fall outside of these regions and are believed to be caused by scattered light in the chamber. All pinholes in the designated regions are included in the LAOP tally. Lastly, POD is calculated for each of these pixels by comparing the incident light falling on that pixel to the light measured in that pixel.

2.3 *Environmental Tests*

The DAM was subjected to vibration and thermal stress to test the durability of the OBF under flight-like environmental stress. The vibration test was performed after the two initial light leak tests (see Fig. 2). The random vibration test was designed to expose the OBF to a vibration environment similar to that experienced during launch. The DAM was tested at 14.1 G's random vibration from 20 to 2000 Hz on each of the three axes separately as specified in Table 2.4–3 in

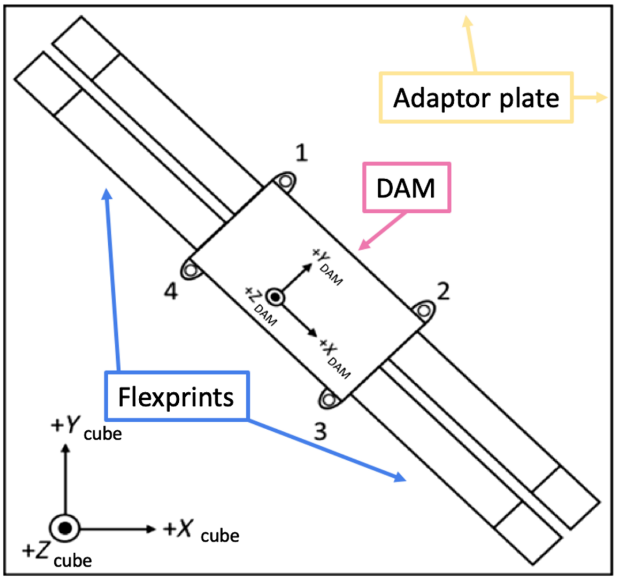

Fig. 6 DAM containing the CCCDs is mounted diagonally on the adaptor plate to allow room for the flexprint cables. Note that the *X* and *Y* test axes (lower left) do not line up with the *X* and *Y* DAM axes.

Ref. 7. A low level white noise random vibe was performed before and after each of the full-level tests to identify the natural frequencies of the system and check for frequency shifts. The vibration level for each axis began at −18 dB relative to the full level, then increased to −12 dB, then −6 dB, and finally the full level test. The detector was not powered during vibration testing. The DAM was mounted to an adaptor plate, and the adaptor plate was mounted to a shake cube in the environmental test facility at Lincoln Laboratory. To accommodate the flexprints safely, the DAM was mounted at a 45-deg angle about the *Z*-axis of the cube, as shown in Fig. 6. The *Z*-axis for the cube and for the DAM were the same while Y_{cube} and X_{cube} were rotated 45 deg from Y_{DAM} and X_{DAM}, respectively. Therefore, when the cube vibrated in the *Y* direction, the DAM experienced vibrations in both the *Y* and *X* directions.

As a result of the light leak testing, the DAM experienced eight thermal cycles encompassing the range −70°C and −50°C with a stability of 1°C/h for at least 1 h. Note that on some cycles the

Table 1 Thermal cycling of the DAM during the tests.

Minimum temperature (°C)	Maximum temperature (°C)	Test performed
−70	−15	Initial light leak test 1
−70	20	Initial light leak test 1
−70	20	Initial light leak test 2 (fiber problems)
−70	20	Initial light leak test 2
−70	0	Postvibration light leak test 1
−70	20	Postvibration light leak test 2
−90	−20	−90°C light leak test 1
−90	20	−90°C light leak test 2
−70	20	Rotated DAM light leak test
−70	20	Post eight thermal cycles light leak test

DAM went warmer or colder, but always included a full cycle around these required instrument operating temperatures. Due to the nature of the light leak tests, the DAM was cooled to at least −70°C once or twice per light leak test and was allowed to stabilize at that temperature for over an hour. Figure 2 shows the timing of each thermal cycle over the course of the environmental testing. The high temperature of each cycle was well above the required instrument operating temperature of −50°C, and Table 1 shows the high and low temperatures of each cycle.

3 Ground Testing Results

To evaluate the impact of the environmental tests on the OBF, we calculated the LAOP for the detector and POD for each pinhole for each set of light leak tests that were performed: initial, postvibration test, and postthermal cycling. The LAOP measures the number of pixels that observed light transmitted through the OBF, and POD measures the amount of light that was transmitted through each pinhole. The LAOP and POD values for the poststress test data sets were assessed to determine if they meet the REXIS science requirements and were compared with LAOP and POD from the initial light leak tests to measure any degradation in the performance of the OBF due to environmental stress. Due to cosmetic defects not related to the OBF, such as hot columns and edge bleed, we were unable to evaluate the pinholes in the OBF in two of the four CCDs in the DAM. In our analysis, we include data from two CCDs (CCD0 and CCD2).

3.1 *Pre-Environmental Pinhole Characterization*

The results of the initial light leak tests conducted before environmental testing confirms the existence of pinholes in the the OBF on the flight spare CCDs, but the number of pinholes meets the REXIS science mission requirements. Figure 7 shows the location and spread of the pinholes in the OBF for CCD0 and CCD2. The red lines indicate the area of each CCD that is illuminated, and pinholes within those areas are the ones used in the analysis. For CCD0, the illuminated area is 527 pixels × 314 pixels, and for CCD2, it is 300 pixels × 514 pixels (for reference each CCD is 1024 pixels × 1024 pixels). Note that pinholes are detected outside of the defined illuminated area, likely due to the scattering of the uncollimated light from the fiber within the chamber. However, only pinholes within the illuminated area are included when calculating LAOP. The initial pre-environmental LAOP for both of the CCDs is well below the REXIS science requirement of 1% of the illuminated area, and the change in LAOP between runs is less than 2σ for both 4.6- and 11.0-mW illumination levels (see Table 2). The number of pixels with POD <7 is also below 1% of the illuminated area and does not vary by more than 2σ between runs.

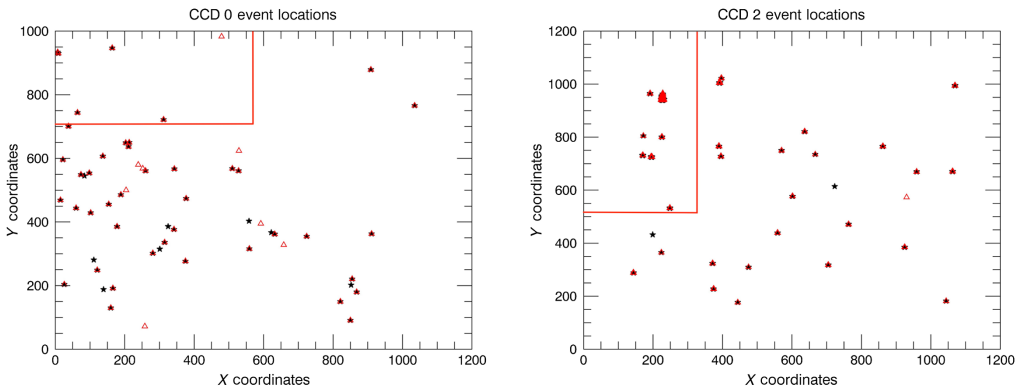

Fig. 7 Locations of the pinholes in CCD0 and CCD2 during the pre-environmental tests at 11.0 mW. Black stars are pinholes from the first light leak test and red triangles are pinholes from the second light leak test. The red lines define the illuminated portion of each of the CCDs. Note that these plots are shown in the readout orientation, so CCD 2 is rotated 180 deg from the physical orientation. Also note that pinholes on adjacent pixels are quite close to each other and may overlap.

Table 2 Initial light leak levels. LAOP for CCD0 and CCD2 at 4.6 and 11.0 mW. The fraction of LAOP pixels is in relation to the total number of pixels in the illuminated region. The $2\sigma_{LAOP}$ for each test that is used to determine test variability is calculated from the average LAOP in this test.

	Optical light (mW)	Test 1		Test 2		Change in LAOP (pixel)	$2\sigma_{LAOP}$
		LAOP	%	LAOP	%		
CCD0	4.6	9	0.01	8	0.01	1	1.4
CCD2	4.6	75	0.05	72	0.05	3	4.2
CCD0	11.0	16	0.01	14	0.01	2	2.8
CCD2	11.0	120	0.08	124	0.08	4	5.6

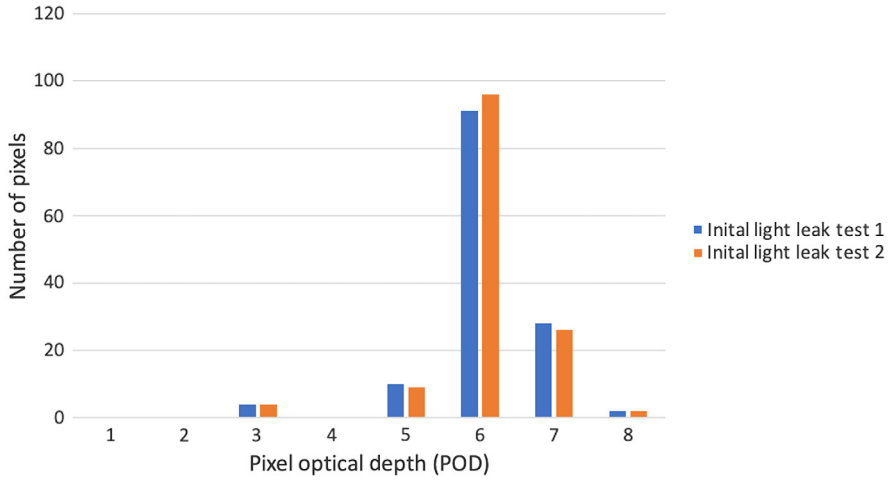

Fig. 8 Pre-environmental POD distribution of the pixels with light leak in the illuminated area at 11.0 mW. Each run shows the combined count from CCD0 and CCD2. The first run had 133 pixels with POD <7 which is 0.04% of the illuminated area. The second run had 135 pixels with POD <7 which is 0.04% of the illuminated area.

The distribution of POD is shown in Fig. 8. Note that there are a few occurrences of a single elevated pixel, but most identified pinholes are clumped in multipixel groups that all have light leak signal. For these groups of pixels, the central pixels have higher signal and lower POD while some of the edge pixels have lower signal and higher POD. Given that the measured physical size of the pinholes, <1 μm, is less than the size of one pixel, 24 μm, it is likely that these areas represent pinholes that are clustered together and are not the result of a large single pinhole that exposes multiple pixels. While the majority of pinholes do have POD <7, the sum is 0.04% of the illuminated area. The pinholes do transmit a significant portion of the incident flux; however, there are few enough that the OBF performance meets the instrument requirements. These results give confidence that the test setup is sufficient to observe any change in LAOP or POD that may indicate deterioration of the OBF.

3.2 *Postvibration Pinhole Characterization*

The results of the light leak tests performed after the vibration test are given in Table 3 and Fig. 10. Both LAOP and POD show little to no change in the OBF performance. The locations of the pinholes before and after the vibration test are shown in Fig. 9 in black and red. The pinholes from this set of tests are shown as red squares and crosses and almost entirely overlap, though there are a few places where a pinhole was only detected in one of the tests. The number

Table 3 Light leak level after the vibration test. LAOP for CCD0 and CCD2 at 4.6 and 11.0 mW. The fraction of LAOP pixels is in relation to the total number of pixels in the illuminated region. $2\sigma_{LAOP}$ is calculated using the pre-environmental light leak average LAOP and represents the variation in the test setup.

	Optical light (mW)	Test 1		Test 2		Change in LAOP (pixel)	$2\sigma_{LAOP}$
		LAOP	%	LAOP	%		
CCD0	4.6	9	0.01	10	0.01	1	1.4
CCD2	4.6	66	0.04	64	0.04	2	2.8
CCD0	11.0	16	0.01	16	0.01	0	1.4
CCD2	11.0	115	0.08	118	0.08	3	4.2

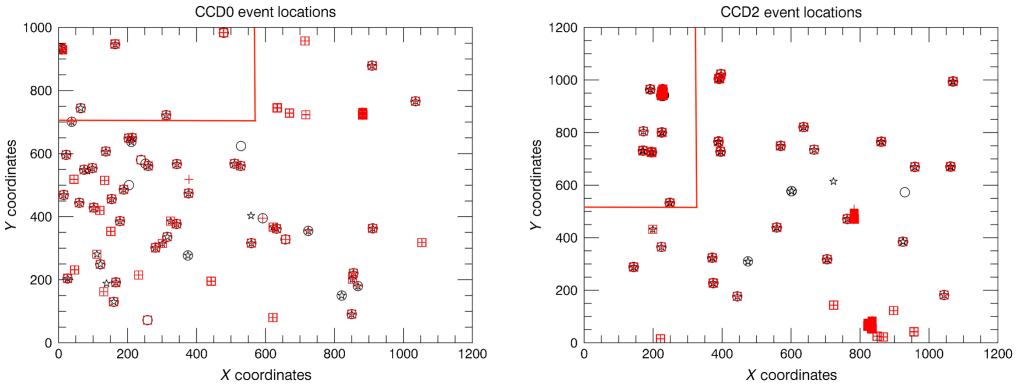

Fig. 9 Locations of the pinholes in CCD0 and CCD2 during the postvibration tests at 11.0 mW in comparison with the pinholes from the initial light leak test. Black stars and circles are pinholes from the two previbration tests and red squares and crosses are pinholes from the two postvibration tests. The red lines define the illuminated portion of each of the CCDs. Note that these plots are shown in the readout orientation, so CCD 2 is rotated 180 deg from the physical orientation. Also note that pinholes on adjacent pixels are quite close to each other and may overlap.

of these variations is presented in the column labeled "change in LAOP" in Table 3. The LAOP for CCD0 is nearly identical to the initial LAOP (within one pixel), whereas the LAOP values for CCD2 decreased between 5 and 8 pixels (see Table 4). This slight variation is well within the 2σ tolerance. The postvibration LAOP is still well below 1% of the total illuminated region. The fraction of pixels with POD <7 postvibration testing is significantly below 1% at 0.04% of the illuminated area. As in the initial light leak tests, the distribution of POD is almost entirely <7 as seen in Fig. 10. The variation in the average total number of pixels with POD <7 between the initial light leak tests and the postvibration light leak tests is also within 2σ.

3.3 *Postthermal Cycling Pinhole Characterization*

Given the repeated stability in previous tests, only one light leak test was performed after eight thermal cycles of the DAM (see the final box in the testing flowchart in Fig. 2). The results of the light leak test after the thermal cycling show that thermal cycling the CCDs did not deteriorate the performance of the OBF. Figure 11 shows the location of the detected pinholes in both CCDs with red crosses. These locations correlate well to pinholes identified in the initial light leak tests (black stars and circles). Table 4 includes the total number of pixels that make up LAOP for each CCD and the LAOP fraction of the total potential pixels, as well as the comparison to the initial light leak test and the postvibration light leak test. After thermal cycling, the calculated LAOP is

Table 4 Change in the average LAOP between the initial light leak test, the post-vibration light leak test, and the post-thermal cycling light leak test. The 2σ value is the tolerance on how much the LAOP could increase and pass the OBF requirements. Both CCDs passed after both environmental stress tests. The LAOP is given both in number of pixels and then in parenthesis as percentage of illuminated area.

	Optical light (mW)	Initial LAOP Avg. (%)	$2\sigma_{LAOP}$	Post-vibe LAOP avg. (%)	Post-thermal LAOP Avg. (%)	Pass/fail
CCD0	4.6	8.5 (0.01)	+2	9.5 (0.01)	6 (0.01)	Pass
CCD2	4.6	73.5 (0.05)	+8	65 (0.04)	60 (0.05)	Pass
CCD0	11.0	15 (0.01)	+3.2	15.5 (0.01)	13 (0.01)	Pass
CCD2	11.0	122 (0.08)	+7	116.5 (0.08)	107 (0.08)	Pass

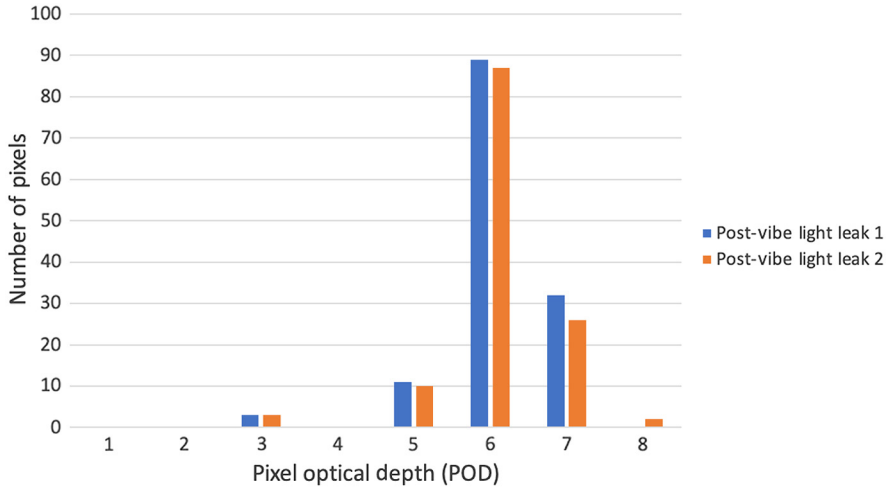

Fig. 10 Postvibration test POD distribution of the pixels with light leak in the illuminated area at 11.0 mW. Each run shows the combined count from CCD0 and CCD2. The first run had 135 pixels with POD <7, which is 0.04% of the illuminated area. The second run had 126 pixels with POD <7, which is 0.04% of the illuminated area.

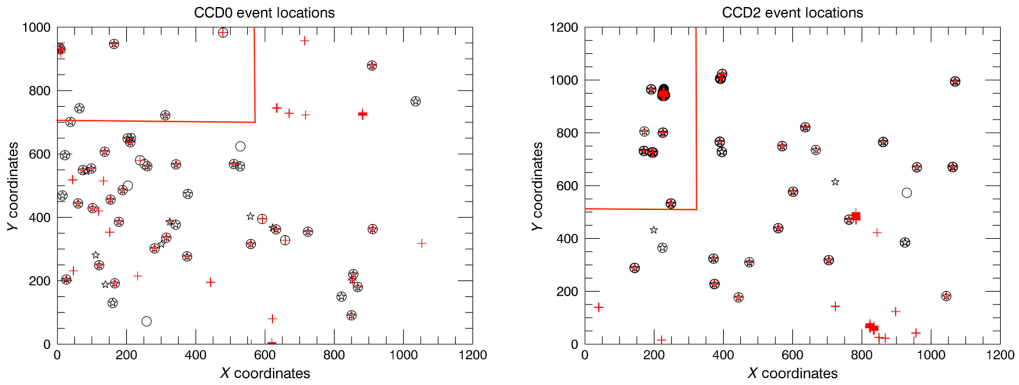

Fig. 11 Locations of the pinholes in CCD0 and CCD2 during the postthermal cycling tests at 11.0 mW in comparison with the pinholes from the initial light leak test. Black stars and circles are pinholes from the two initial light leak tests and red crosses are pinholes from the postthermal cycling test. The red lines define the illuminated portion of each of the CCDs. Note that these plots are shown in the readout orientation, so CCD 2 is rotated 180 deg from the physical orientation. Also note that pinholes on adjacent pixels are quite close to each other and may overlap.

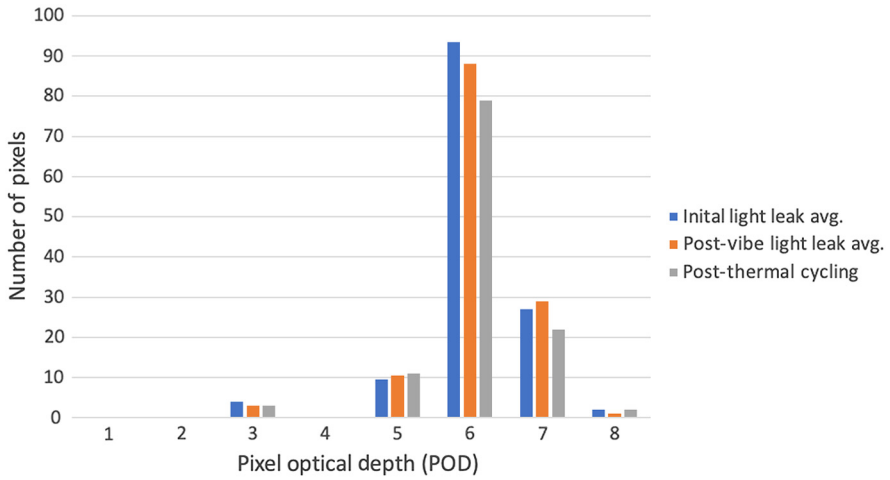

Fig. 12 A comparison of the POD distribution of pixels with light leak in the illuminated area at 11.0 mW from the initial light leak tests, postvibe light leak tests, and postthermal cycling test. The combined count from CCD0 and CCD2 is shown. The postthermal cycling data have 115 pixels with POD <7, which is 0.04% of the illuminated area.

significantly below 1% of the illuminated area. The CCDs at both illumination levels have LAOP within 2σ of the initial LAOP. The total combined number of pixels with POD <7 is 117, fewer than the 135 found in the initial light leak test. Figure 12 shows the comparison of the POD levels for the initial, postvibration test, and postthermal cycling light leak tests. Both metrics (LAOP and POD <7) decreased, which indicates that any variation present between tests is likely due to variability of the testing system and not from a physical deterioration of the OBF.

4 OBF Characterization in Flight Data

Characterization of the flight OBF is possible using the in-flight data. We consider the OBF performance in two stages: first, with the radiation cover closed during the 2-year cruise to the asteroid (when nearly all optical light was blocked), and then again once the radiation cover was opened and optical light from Bennu is incident on the CCD array. The data with the cover closed are analyzed to identify all pixels with regular levels of excess charge. These "hot pixels" have elevated levels of dark current in the absence of incident photons. A similar analysis is then performed on the data taken with the cover open and Bennu in the field of view (FoV). Pixels that show repeated levels of excess charge only in the cover open configuration are assumed to be caused by pinholes in the flight DAM's OBF.

A variety of factors in the flight DAM's performance can influence our ability to characterize the flight OBF. A light leak through the uncoated edge of the CCDs, where the bond wires are located, was observed after the radiation cover was opened in September of 2018.[9] This light leak is independent of the performance of the OBF but does limit our ability to evaluate the OBF performance in the flight data. We have calculated a lower limit on the LAOP for the flight OBF but were not able to calculate POD for any of the pixels. Due to hardware complications before launch and noise issues in flight, only six of the original 16 nodes in the DAM were enabled and working.[10] Our discussion of the OBF performance in flight uses data from these six functional nodes.

REXIS CCD data products consist of raw frames, bias maps (generated by median-averaging 10 raw frames), and event list data. The event list is the primary REXIS CCD data product and is produced by on-board processing of the frames to identify x-ray events.[11] Briefly, the onboard processing subtracts the bias map from a raw frame to remove noise and systematics, and pixels with collected charge above an "event threshold" are recorded as events. The location, number of neighboring pixels with significant charge, and total charge of these events are calculated and downlinked from REXIS in the form of an event list. The on-board processing has the ability to use an optional hot pixel mask (HPM), a list of pixels to ignore when analyzing the frames to

build the event list. In this way, we can ignore pixels with elevated dark current or pixels affected by OBF pinholes when creating the x-ray event list.

4.1 *Hot Pixel Identification*

Upon arrival of the OSIRIS-REx spacecraft at Bennu, but before REXIS began science observations, we collected two sets of calibration data with the sun-illuminated asteroid in the CCD FoV to characterize the instrument response in the presence of reflected light and identify pinholes. During the Launch+30 month (L+30) operation in February 2019, REXIS downlinked a CCD bias map, two raw frames, and 15 min of event list data. These data were used to generate a preliminary HPM, which was tested during the OBF verification operation in June 2019. During this observation, REXIS collected two raw frames, two bias maps, 1 h of event-list data with no HPM, and 1 h of event-list data using the preliminary HPM from the L+30 data. The data from the OBF verification were used to update the list of hot pixels.

We constructed a list of hot pixels by considering the amount of charge collected by each pixel in the two raw frames and the bias map. The distribution of these values in the bias map is shown in Fig. 13. We generated a preliminary HPM by placing a threshold on the charge value for each pixel; pixels that exceeded this value in both the raw frames and the bias map were considered hot. Since the number of pixels in the HPM is limited by the number of commands that can be uplinked to the spacecraft (subject to change from one operation to the next), the threshold value is tuned to generate a list of hot pixels that fits within the time allotted to REXIS for instrument commanding. We identified 456 pixels with collected charge greater than this threshold in both raw frames and the bias map.

We used the event-list data to verify that the HPM performed as expected. The event-list data with no HPM had several pixels that recorded multiple events; all of these "hot" pixels were in the HPM from the L+30 data. In the event-list data with the HPM applied, some pixels adjacent to the "hot" pixels recorded multiple events. When adjacent pixels record an event, the charge from both pixels is added, and the event list only records the position of the pixel with the greater charge. Since the limit on the number of hot pixel commands was expanded for subsequent operations, we regenerated the HPM with a reduced threshold and used a list of 1234 pixels in the HPM for subsequent REXIS operations.

Figure 14 shows a bias map from the OBF Verification; the 1234 pixels that were included in the HPM are marked with cyan circles. These 1234 hot pixels identified out of the 154,250 pixels

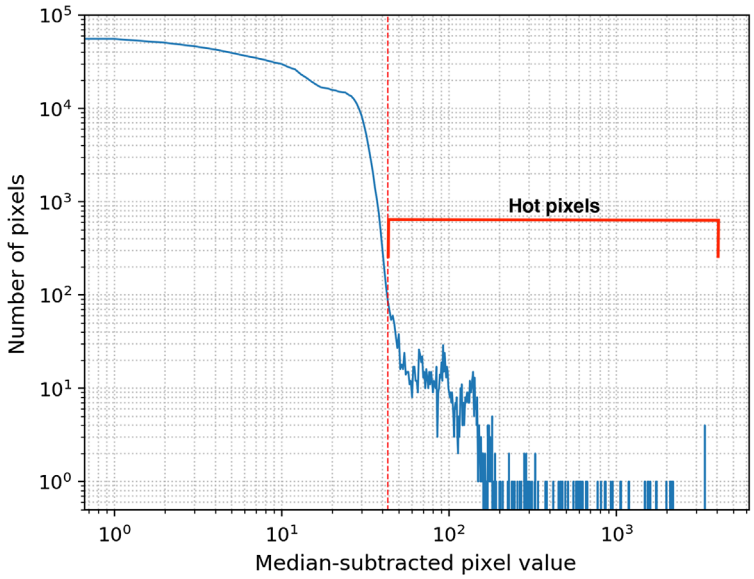

Fig. 13 A histogram of the pixel values in the six good nodes from the bias map taken during L+30. The dashed red line indicates the charge threshold used to identify hot pixels. The units on the *x* axis are arbitrary units of pixel charge.

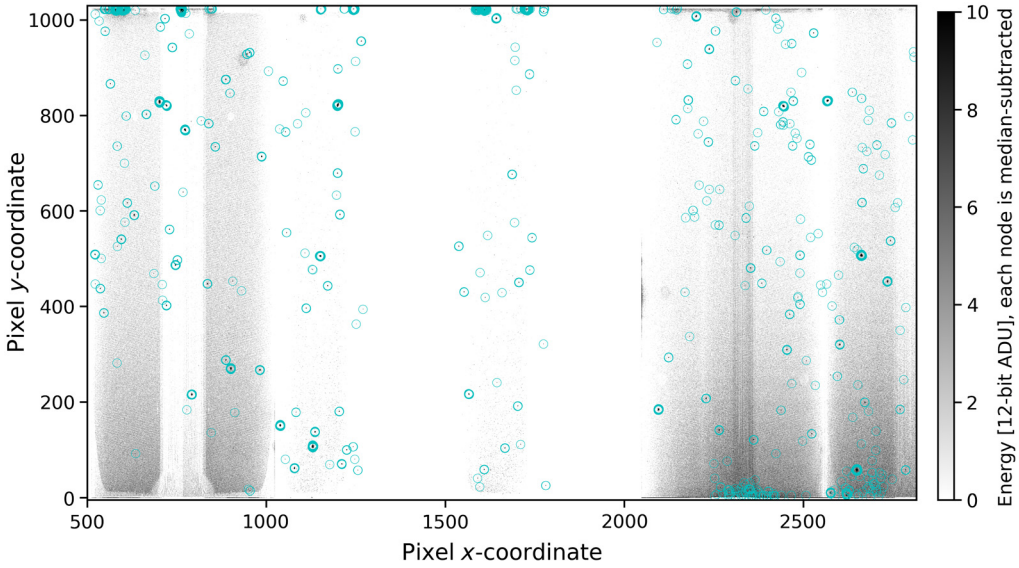

Fig. 14 A bias map from the OBF verification data. The gray scale indicates the charge collected by each pixel, and the cyan circles denote hot pixels that were included in the HPM. Some detector nodes were disabled for this operation, which causes gaps in the data from *x*-coordinate 1280 to 1536 and 1792 to 2048. Note, the detector nodes are arranged in their readout order, not in their physical layout in the detector array. The readout edge of each node is located at the bottom of the figure; and the vertical gradient in the pixel energy is due to the light leak around the edge of the detector.

in the active detector area provide an estimate of the LAOP in the flight DAM. The flight LAOP is only 0.08% of the detector area, well below the science requirement that LAOP is no larger than 1% of the illuminated area.

4.2 *Science Operations in the Presence of Optical Light*

REXIS collected a total of 617 h of data during science operations which were all conducted from a low altitude polar terminator orbit around the asteroid Bennu at an altitude between 700 m and 1 km from the surface. These data were taken during two separate intervals, each about 1 month in duration: the first beginning in July 2019, and the second beginning in November 2019. Although a clear x-ray signal from the asteroid has not been resolved[12] from these data, REXIS did make unambiguous detections of a number of astrophysical x-ray sources at the edge of its FoV. During these observations, 90% of the REXIS FoV were subtended by the asteroid with a small section of the sky visible around the limb of the asteroid at all times, enabling the observation of the x-ray sky at the asteroid horizon. Within this narrow region, the detection of astrophysical sources was achieved; the brightest of these include Cyngus X-1 and Cygnus X-2, well-known galactic high mass x-ray binaries, and MAXI J0637-430,[13,14] a new transient low mass x-ray binary initially detected by the Monitoring of All-Sky X-ray Image (MAXI) telescope onboard the International Space Station (ISS)[15] just a few days prior to the start of REXIS's second observing period. The ability to detect and characterize the variability of these sources in the presence of the bright asteroid (Bennu), which continually illuminated the CCDs over the course of these observations, definitively demonstrates the effectiveness and durability of the directly deposited OBF used in the construction of the REXIS instrument which made these observations possible.

5 Conclusion

The aim of the ground environmental testing on the flight spare hardware was to determine whether the performance of the newly developed directly deposited OBF on the REXIS

CCDs would degrade due to the vibrational stresses of launch and the thermal environment in space. Our tests demonstrate that the technology can be raised to TRL 6. Given that no deterioration of the OBF was measured over the course of the environmental testing on the ground and the OBF performance in flight, Lincoln Laboratory's method of directly depositing an aluminum OBF onto the surface of a CCD is able to withstand stresses of launch and an extended life-mission in the space environment and can be classified as TRL 9 for interplanetary x-ray observations. From the observations in the light environment of the asteroid, it is shown that this method of blocking optical light successfully enabled a mission such as REXIS to observe in the soft x-ray energy band without excessive optical light contamination.

Acknowledgments

This work was conducted under the support of the OSIRIS-REx program through research funds from Goddard Space Flight Center. REXIS would not have been possible without supporting expertise, facilities, and mentorship at MIT Kavli Institute provided by Marshall W. Bautz and at MIT Lincoln Laboratories provided by Kevin Ryu, Keith Warner, Jim Kelly, Joe Orrender, Jeff Mendenhall, Marc Bernstein, and others. The work here was sponsored by NASA's Strategic Astrophysics Technology Program Grant No. NNX12AF22G to MIT and corresponding IPR NNH12AU04I to Lincoln Laboratory. MIT Lincoln Laboratory material is based upon work supported by the United States Air Force under Air Force Contract No. FA8702-15-D-0001. Any opinions, findings, conclusions, or recommendations expressed in this material are those of the author(s) and do not necessarily reflect the views of the United States Air Force.

References

1. D. Lauretta et al., "OSIRIS-REx: sample return from asteroid (101955) Bennu," *Space Sci. Rev.* **212**, 925–984 (2017).
2. R. A. Masterson et al., "Regolith X-Ray Imaging Spectrometer (REXIS) aboard the OSIRIS-REx asteroid sample return mission," *Space Sci. Rev.* **214**, 48 (2018).
3. K. Ryu et al., "Directly deposited optical-blocking filters for single-photon x-ray spectroscopy," *J. Astron. Telesc. Instrum. Syst.* **3**, 036001 (2014).
4. T. Tanaka et al., "Soft X-ray Imager aboard Hitomi (ASTRO-H)," *J. Astron. Telesc. Instrum. Syst.* **4**(1), 011211 (2018).
5. H. Tomida et al., "Solid state slit camera (SSC) of the MAXI mission for JEM (Japanese Experiment Module) on the International Space Station (ISS)," *Proc. SPIE* **4140**, 304–312 (2000).
6. M. Jones et al., "Engineering design of the regolith x-ray imaging spectrometer (REXIS) instrument: an OSIRIS-REx student collaboration," *Proc. SPIE* **9144**, 716–731 (2014).
7. "General Environmental Verification Standard (GEVS): for GSFC flight programs and projects," Tech. Rep. GSFC-STD-7000A, NASA Goddard Space Flight Center (2019).
8. *NASA systems engineering processes and requirements*, Tech. Rep. NPR 7123.1C, NASA, Washington, DC (2020).
9. M. Lambert, "A root cause analysis of REXIS detection efficiency loss during phase E operations," MIT Department of Aeronautics and Astronautics Master's Thesis, MIT University Press, Cambridge (2020).
10. J. Hong et al., "Calibration and performance of the REgolith X-Ray1Imaging Spectrometer (REXIS) aboard NASA's2OSIRIS-REx mission to Bennu," *Space Sci. Rev.* **217**(8) (2021).
11. P. Biswas, "Radiation management, avionics development, and integrated testing of a class-D space-based asteroid x-ray spectrometer," MIT Department of Aeronautics and Astronautics Master's Thesis, MIT University Press, Cambridge (2016).
12. D. Hoak et al., "Observations of 101955 Bennu with the Regolith X-ray imaging spectrometer," in preparation (2021).
13. B. Allen et al., "Detection of MAXI J0637-430 by the REgolith X-Ray Imaging Spectrometer (REXIS) onboard OSIRIS-REx," Astronomer's Telegram, [ATel 13594] (2020).

14. B. Allen et al., "Detection and characterization of x-ray sources around the limb of an asteroid using modified back-projection imaging with the regolith x-ray imaging spectrometer on-board osiris-rex," in preparation (2021).
15. M. Matsuoka et al., "The MAXI mission on the ISS: science and instruments for monitoring all-sky x-ray images," *Publ. Astron. Soc. Jpn.* **61**, 999 (2009).

Carolyn Thayer is currently a master's student in space engineering in the Climate and Space Sciences and Engineering Department at the University of Michigan. She received her BA degree in astronomy from Wellesley College in 2014. Between undergrad and grad school, she worked for 6 years as a test engineer at the MIT Kavli Institute, where she also worked on REXIS.

Rebecca Masterson is a principal research scientist at MIT and director of the MIT Space Systems Laboratory. She holds affiliations with both the Department of Aeronautics and Astronautics and the MIT Kavli Institute. She has over 20 years of experience in spacecraft and instrument development, including structural design, control structure interactions, system engineering and integration and test. She was the instrument manager for REXIS.

Branden Allen is a senior research scientist at the Harvard College Observatory, part of the Center for Astrophysics, Harvard-Smithsonian. He has over 20 years of experience in the development, deployment, and operation of ground, balloon, and spaceflight scientific instrumentation/systems and methods for cosmic ray/particle-astrophysics, x/gamma-ray astronomy and, most recently, planetary science.

Kevin Ryu is a technical staff member in the Advanced Imager Technology Group at MIT Lincoln Laboratory. His expertise centers on device physics, fabrication, and modeling. He has led the microfabrication of single-photon x-ray imaging spectroscopy CCDs for REXIS. He received his PhD from MIT in electrical engineering and computer science.

Mark Chodas is currently a systems engineer at the NASA Jet Propulsion Laboratory. Before joining JPL, he received his SB, SM, and PhD degrees in aeronautics and astronautics from Massachusetts Institute of Technology. While at MIT, he was the systems engineer for the REXIS instrument.

Jaesub Hong is a senior research scientist at Harvard University and has over 20 years of experience in development of soft and hard x-ray telescopes for high energy astrophysics and planetary science. He was an instrument scientist for REXIS and was deputy-PI for a mission concept study for CubeSat X-ray Telescope (CubeX). His research includes the development of advanced hard x-ray detectors and lightweight x-ray mirrors for future x-ray telescopes in astrophysics and planetary science.

Madeline Lambert is currently an operations systems engineer at the NASA Jet Propulsion Laboratory. She received her bachelor's degree in physics from the University of Wisconsin - La Crosse and her master's degree in aeronautics and astronautics from Massachusetts Institute of Technology. While at MIT, she was the instrument operations engineer for REXIS.

Jonathan Grindlay is the Robert Treat Paine professor of astronomy at Harvard. His primary interests are time-domain astrophysics of accreting black holes and exploring their populations, formation, and evolution with wide-field coded aperture x-ray/gamma-ray imaging and spectra.

Richard P. Binzel is a professor of planetary science and joint professor of aerospace engineering at Massachusetts Institute of Technology. His scientific analysis has shown the link between major meteorite groups and their formation and source locations. He is a coinvestigator on NASA's OSIRIS-REx asteroid sample return mission and PI of REXIS.